CrossMark

The magma plumbing system of Bezymianny Volcano: Insights from a 54 year time series of trace element whole-rock geochemistry and amphibole compositions

Stephen J. Turner [a,*], Pavel Izbekov [b], Charles Langmuir [a]

[a] Department of Earth and Planetary Sciences, Harvard University, United States
[b] Geophysical Institute, University of Alaska Fairbanks, United States

ARTICLE INFO

ABSTRACT

Samples from 33 individual eruptions of Bezymianny volcano between 1956 and 2010 provide an opportunity to study in detail the temporal evolution of an arc volcano. Major element and ICP-MS trace element analyses show that the eruptive products shifted progressively from relatively silicic magma in 1956 (~60.4% SiO_2) to more mafic compositions (e.g. 56.8% SiO_2 in 2010). Amphibole compositions changed concurrently from low-Al_2O_3 to high-Al_2O_3. Whole rock element-element variation diagrams show tight compositional arrays, some with a distinct kink in the late 1970s, which cannot be reproduced by fractionation of a single magma along a liquid line of descent. Amphibole thermobarometry indicates amphibole crystallization in two separate reservoirs, one between 200 and 300 MPa, and another between 500 and 750 MPa. Liquid compositions calculated from the amphibole analyses show that liquids stored in each reservoir become increasingly mafic from 1956 to 2010, suggesting that each reservoir received magma inputs from more mafic sources throughout the eruptive cycle.

End member mixing analysis of the dataset allows calculation of three end member compositions that can be combined in varying proportions to reproduce major and trace element whole rock compositions. The end-member mixing proportions vary systematically between 1956 and 2010, with maxima for end-members A, B and C during 1956, 1977, and 2010, respectively. Major element compositions of phenocrysts, combined with published trace element partition coefficients, show that each end member may have evolved from a common parental magma by fractionation of three different mineral assemblages, possibly due to different pressures of crystallization and volatile contents. The petrologic data are consistent with three magma reservoirs at different depths. Magmas from the shallowest reservoir erupted first, with increasing proportions of deeper reservoirs over time. Past studies have demonstrated similarities in eruptive style between Bezymianny and both Mount St. Helens and Soufrière Hills volcanoes. Contrasting time series data show that the magma plumbing systems of Mount St. Helens and Bezymianny have little in common, while Soufrière Hills may be a better analog. Similar eruptive styles at the surface do not necessarily reflect similar systems of magma supply and evolution at depth.

© 2013 Elsevier B.V. All rights reserved.

1. Introduction

The composition of a magma erupted at an arc volcano is a function of the source composition, the extent of melting, the pressure and temperature conditions in which the magma undergoes fractional crystallization, and the extent to which that magma has mixed with crustal material and other batches of magma and crystals during its ascent from the mantle. Regional and global studies have advanced our understanding of the physical mechanisms that control the source composition, extent of melting, and extent of crustal assimilation at volcanic arcs (e.g. Hildreth and Moorbath, 1988; Plank and Langmuir, 1988; Elliott et al., 1997; Class et al., 2000). Polybaric crystal fractionation and magma mixing are more difficult to detect

in regional studies, which have large spatial coverage, but poor spatial and temporal resolution. Evidence for these processes primarily comes from detailed studies of individual volcanic centers (e.g. Grove et al., 2005), though it is probable that such processes affect a large portion of erupted arc magmas (Sparks et al., 1977; Eichelberger et al., 2006; Kent et al., 2010). A complete understanding of volcanic arcs, therefore, must include careful examinations of the magma supply systems of individual volcanoes. Frequently erupting volcanoes, such as Bezymianny, are valuable natural laboratories in which these processes can be investigated.

This study provides an extensive, high-quality data set on a series of samples for which the time of eruption is known precisely, within the course of 54 years of eruptions at Bezymianny volcano. The primary goal of this work is to understand the processes responsible for such short term compositional variations. The duration of the eruptive activity at Bezymianny coupled with the high temporal resolution

---

* Corresponding author.
E-mail address: sturner@fas.harvard.edu (S.J. Turner).

of sampling is unprecedented, allowing new insights to be drawn from analyses of both whole rock and amphibole compositions. Continuous variations in erupted whole rock compositions at Bezymianny clearly demonstrate multi-component magma mixing. These whole rock compositional variations, augmented by themobarometric and chemometric constraints from amphibole compositions, enable quantitative modeling of the compositions of mixing components as well as the pressure and temperature conditions of the reservoirs that contain them. The dense temporal sampling of the eruptive products of Bezymianny provides a unique opportunity to understand how the relative proportions of mixing components have varied through time, from which a robust physical model of the volcano's plumbing system can be constructed.

Similar case studies have been conducted at a few other volcanoes. At Arenal volcano in Costa Rica, mineral analysis indicates multiple episodes of basaltic replenishment have occurred over the course of 30 years, despite nearly constant bulk rock compositions (Streck et al., 2002). Eruptive products from the beginning of the 1996 eruption of Karymsky volcano, in Kamchatka, have a basaltic signature in both glass and mineral chemistry. Within a few months after the initial eruption, however, the basaltic signature diminished, and the composition of erupted material remained nearly constant for the following three years (Izbekov et al., 2004). At Mount St. Helens, bulk rock compositions have varied somewhat among recent eruptions, but there is no evidence for an influx of new mafic magma (Pallister et al., 2008). Bezymianny provides an additional case study that contributes to our understanding of the diversity of time-series data from active volcanoes.

2. Geological background and recent eruptive history of Bezymianny Volcano

Bezymianny volcano is a member of the Kliuchevskoi group of volcanoes, situated within the Central Kamchatka Depression (CKD). The volcano is located on the southern flank of the older and presumably extinct Kamen volcano, which in turn is immediately south of Kliuchevskoi volcano, the largest and most active volcanic center in the CKD. Bezymianny began growing approximately 10,000–11,000 yr BP, with extended repose periods from 6900 to 4700 BP, 2750 to 2100 BP, 1550 to 1200 BP, and most recently from 1000 BP to 1955 AD (Braitseva et al., 1991). The pre-historic eruptive activity at Bezymianny formed extensive pyroclastic flow deposits, lava flows, and extrusive domes (Braitseva et al., 1991), with magma compositions varying from basaltic to andesitic (e.g. Bogoyavlenskaya et al., 1991; Malyshev, 2000). Basalts are the most common eruptive products of the Kliuchevskoi group of volcanoes, and dacites are rare. In the Holocene, dacites erupted almost exclusively at Bezymianny volcano as well as at several extrusive domes situated along a narrow, longitudinally-oriented fault zone extending from Bezymianny to the south (Timerbaeva, 1967; Melekestsev et al., 1991).

The current eruptive cycle of Bezymianny volcano began in late 1955, when moderate explosive activity and dome growth ended a ca. 1000 year dormancy. On March 30, 1956, within six months of the initial intermittent eruptive activity at the central vent, the eastern flank of Bezymianny suddenly collapsed, generating a massive directed blast followed by four hours of vigorous explosive activity. During this event, the eruptive cloud reached an elevation of 35–40 km, pyroclastic flows devastated an area of ca. 40 km^2, and melting of snow generated lahars as long as 100 km. The climactic eruption destroyed the summit of Bezymianny and formed a 1.3-km-wide crater. Within weeks, the volcano started rebuilding its edifice via extrusion of a dome in the middle of the crater, periodic dome collapses, and associated block-and-ash flows. This type of activity continued until the mid 1970s, at which point the extrusive dome growth continued, complemented by short explosive events generating ash clouds as well as pyroclastic flows and surges, which

were often followed by effusions of lava flows. Between 2000 and 2010, Bezymianny typically erupted twice per year. Girina (this issue) provides detailed accounts of the recent eruptive activity of Bezymianny.

3. Samples and analytical techniques

The sample suite consists of 55 fragments of volcanic bombs, juvenile clasts from pyroclastic flows, lava flows, and two samples of volcanic ash. The collection spans the entire 1955–2010 period of the eruptive activity at Bezymianny and includes samples from 33 individual eruptions. Samples of the most recent eruptions were collected during 2005–2010 summer field work as part of the NSF-funded PIRE project. Samples from earlier periods were provided by Genrietta E. Bogoyavlenskaya, Boris V. Ivanov, Alexander P. Maximov, Alexander and Marina Belousovs, Olga A. Girina, and Phillip Kyle. Extreme care was taken in the identification of juvenile material in pyroclastic deposits. The majority of our samples were collected soon after the cessation of individual eruptive episodes, when the deposits were still hot and could be identified unequivocally. The juvenile blocks in the deposits of pyroclastic density currents were identified based on evidence of their cooling and expansion in situ. A detailed description of samples can be found in Electronic Appendix 1.

The eruptive products of Bezymianny are remarkably homogenous and rarely contain enclaves or xenoliths. A few mafic enclaves have been found in the juvenile material of the 1997 and 2007 eruptions, two of which are included in this study. The juvenile products of the December 2009 and June 2010 eruptions are notable, as they contain abundant light-colored amphibole-bearing enclaves, four of which are included in this study as well. All enclaves appear texturally and compositionally homogenous.

3.1. Analysis of whole rock major and trace element composition

For whole rock analysis, samples were crushed to small chips using a geologic hammer and then pulverized by either an agate mortar or a shatter box with alumina ceramic crucible. Major elements were analyzed by X-ray fluorescence analysis using a PANalytical Axios wavelength dispersive spectrometer at the Advanced Instrumentation Laboratory of the University of Alaska Fairbanks. The instrument was calibrated at the beginning of analytical session using AGV-1 BHVO-1, BIR-1, JB-2, JGb-1, JP-1, and JR-1 standard reference materials, prepared as glass disks following the same procedure used for samples with unknown concentrations. Trace elements were analyzed by solution nebulized inductively coupled plasma mass spectrometry (SN-ICP-MS) at Harvard University, following digestion in an HF:HNO$_3$ mixture. Measurements were obtained using a Thermo X Series quadruple mass spectrometer. Standard powders BHVO-2, DNC-1, JB-2, W-2, and BCR-2 were used to generate calibration curves. The full description of sample preparation, analytical conditions, and uncertainties of measurements can be found in the Electronic Appendix 2.

3.2. Electron microprobe analysis of amphiboles

For electron probe microanalysis, all rock samples were prepared as standard petrographic thin sections, polished, and carbon-coated to a thickness of ca. 250 Å. Amphiboles were analyzed for major elements at the University of Alaska Fairbanks using a Cameca SX-50 electron microprobe, which is equipped with four wavelength-dispersive and one energy-dispersive spectrometers. The electron probe is fully automated with Probe for Windows software (Donovan et al., 2007). A 15 keV, 10 nA, 1–3 μm diameter focused electron beam was used for all analyses. Major oxides are reported in wt.% with Fe$_2$O$_3$ calculated using Probe Amph v.3 (Tindle and Webb, 1994) following stoichiometric considerations of Rock and Leake (1984).

Details about counting times, standards, and typical analytical errors calculated using the methods of Scott et al. (1995) can be found in the Electronic Appendix 2.

4. Results

Bezymianny magmas that erupted during the pre-climactic period in late 1955 and early 1956, as well as magmas of the March 30, 1956 climactic eruption contain (in order of decreasing abundance) phenocrysts of plagioclase, amphibole, orthopyroxene, magnetite, ilmenite, and clinopyroxene, as well as subordinate amounts of quartz and apatite. The erupted material typically contains 35% to 45% phenocrysts and 32% to 42% glass by volume, estimated on a vesicle-free basis.

Plagioclase phenocrysts comprise 35–40 vol.% of Bezymianny andesites and are strongly zoned. A typical plagioclase core-to-rim compositional profile is comprised of (sequentially): An50–60 oscillatory zoning, a dissolution boundary, an abrupt jump in An content up to 70–75 mol%, and a gradual return to An50–60. Less commonly, the dissolution boundary is followed by a resorption zone made of An80–85 plagioclase and abundant melt inclusions. Individual plagioclase phenocrysts often contain multiple iterations of this sequence (Shcherbakov et al., 2011).

The abundance of amphibole decreased rapidly after the climactic March 30, 1956 eruption, diminishing from about 25–30% of all phenocrysts in 1956, to trace quantities in the 1970s. Amphibole can still be found in later eruptive products as resorbed cores in opacitic microcrystalline aggregates of pyroxenes, magnetite, and plagioclase. The relative abundance of clinopyroxene gradually increased through time. Pyroxenes are euhedral and occur as phenocrysts, microphenocrysts, and microlites. The other crystalline phases remained relatively constant across all samples. Titanomagnetites are typically subhedral and occur as microphenocrysts and microlites.

The mafic enclaves from the 1997 and 2007 eruptive products vary in size from a few to tens of centimeters. They are characterized by a rounded shape and concentric textural zoning with vesicular interiors and massive, fine-grained rims. The mafic enclaves are phenocryst-poor, but contain abundant acicular microphenocrysts and microlites of plagioclase, orthopyroxene, clinopyroxene, high-Al amphiboles, and occasional resorbed grains of olivine.

The light-colored enclaves from the 2009 and 2010 eruptive products vary in size from tens of centimeters to 0.5 m. They are irregularly shaped and typically have straight, sharp margins. Their mineral assemblage is similar to that of the host andesite, though they contain a larger proportion of amphibole.

4.1. Range and temporal variation of whole rock compositions

Key major and trace element concentrations are shown in Figs. 1 and 2, with representative analyses in Table 1 (full data tables can be found in Electronic Appendix 3). The samples are all andesitic in composition, and have become increasingly mafic through time, shifting from ~61 wt.% SiO_2 and ~2.5 wt.% MgO in 1956 to ~57% SiO_2 and ~4 wt.% MgO in 2010. All samples have subduction zone trace element patterns, with enrichments in fluid mobile elements (Rb, Ba, Sr, U, Pb) relative to rare earth elements (REE) and relative depletions in high field strength elements (HFSE). Incompatible element concentrations have decreased almost continuously since 1956 (e.g., Fig. 3c). Enrichments of light rare earth elements (LREE) over heavy rare earth elements (HREE) also decreased between 1956 and 2010, with La/Yb dropping from an average of 4.57 to 3.64 (Fig. 3d). While most of the moderately compatible and compatible elements have either increased in concentration or remained constant since 1956, Cr and Ni exhibit more complex behavior. Cr and Ni concentrations increased from an average of 12.6 ppm and 6.7 ppm, respectively, in 1956 to over 2 times these concentrations in 1977 (Fig. 3a–b). From 1977 to 2010, however, Cr concentrations decreased while Ni concentrations remained constant.

The trace element compositions of the light enclaves, which were erupted in 2009 and 2010, are tightly clustered (Fig. 2a). They are enriched in incompatible elements relative to their host magmas and are similar in all trace element concentrations to magmas erupted approximately 10 to 20 years earlier (Fig. 3). The two dark enclaves, which were erupted in 1997 and 2007, are significantly more mafic (basaltic andesite) and have lower concentrations of highly incompatible elements than their host magmas, but higher concentrations of HREE. The average La/Yb ratio of the dark enclaves is 3.1 (Fig. 2b).

The sample compositions form linear arrays on most element–element variation diagrams (Fig. 4d). On some element–element or element–ratio plots, however, there is a "kink" in the arrays that consistently occurs around the points representing the eruptive products of 1977 (Fig. 4a–c). On the linear plots, dark enclaves are generally co-linear with the rest of the samples. On the diagrams showing kinked arrays, the dark enclaves are close to co-linear with samples from the eruptions between 1979 and 2010, though one of the two dark enclaves (09IPE67/1) is slightly offset from this line for some elements.

If the compositional trends at Bezymianny are a fractionation trend, or liquid line of descent (LLD), then the kinks could be generated by the onset of crystallization of some phase at about 3.5 wt.% MgO. It is also possible that the compositional trends are the result of mixing between distinct end-member compositions. In this case, an abrupt change in mixing end members would be necessary in 1977 in order to explain why the compositional arrays kink at this point.

4.2. Range and temporal variation of amphibole compositions

Amphibole comprises up to 30% of all phenocrysts in the pre-climactic ash of Bezymianny and in the andesites of the March 30, 1956 eruption. Amphibole occurs as euhedral prismatic phenocrysts and micro-phenocrysts surrounded by microcrystalline opacitic rims, with widths varying from a few to nearly 50 μm (Plechov et al., 2008). The majority of amphiboles in the pre-climactic ash are texturally and compositionally homogeneous. Their Al_2O_3 content is unimodal and ranges from 8 to 12.4 wt.% (Fig. 5a). In contrast, amphiboles from the climactic eruption show wider compositional variations and vary from 9% to 15% Al_2O_3. High-Al amphiboles are often darker and occur as anhedral cores surrounded by light-colored, low-Al rims (Fig. 6). The boundary between high-Al cores and low-Al rims is sharp, exhibiting a distinctive compositional discontinuity.

The abundance of amphiboles in Bezymianny magmas rapidly declined after the 1956 climactic event. Nevertheless, they can still be found in almost all juvenile products, including the most recent ones. In these recent samples, amphiboles occur as rare resorbed cores in 1–2 mm long opacitic aggregates of plagioclase, pyroxenes, and magnetite microlites. Although the range of compositional variations in the post-climactic amphiboles remained nearly the same as in the March 30, 1956 magma, high-Al amphiboles became more abundant with time (Fig. 5b–c).

Our amphibole analyses confirm the results of previous studies for the 1956 magma, which report compositions predominantly within the ranges of magnesio-hastingite and tschermakite (Al'meev et al., 2002; Plechov et al., 2008). The addition of amphibole data for the post-1956 period, however, indicates a somewhat broader range of compositions in addition to systematic temporal variation. Al_2O_3 concentrations, for example, vary from 8.47 wt.% to 14.65 wt.%, while Na_2O compositions vary from 1.49 wt.% to 2.62 wt.%. Lower Al_2O_3 amphiboles are more abundant in the earlier eruptive products and are scarce in all eruptive products after the 1970s. The amphibole compositions also appear to vary bimodally, with one cluster around 9 to 10 wt.% Al_2O_3 and another around 13 to 14 wt.% Al_2O_3.
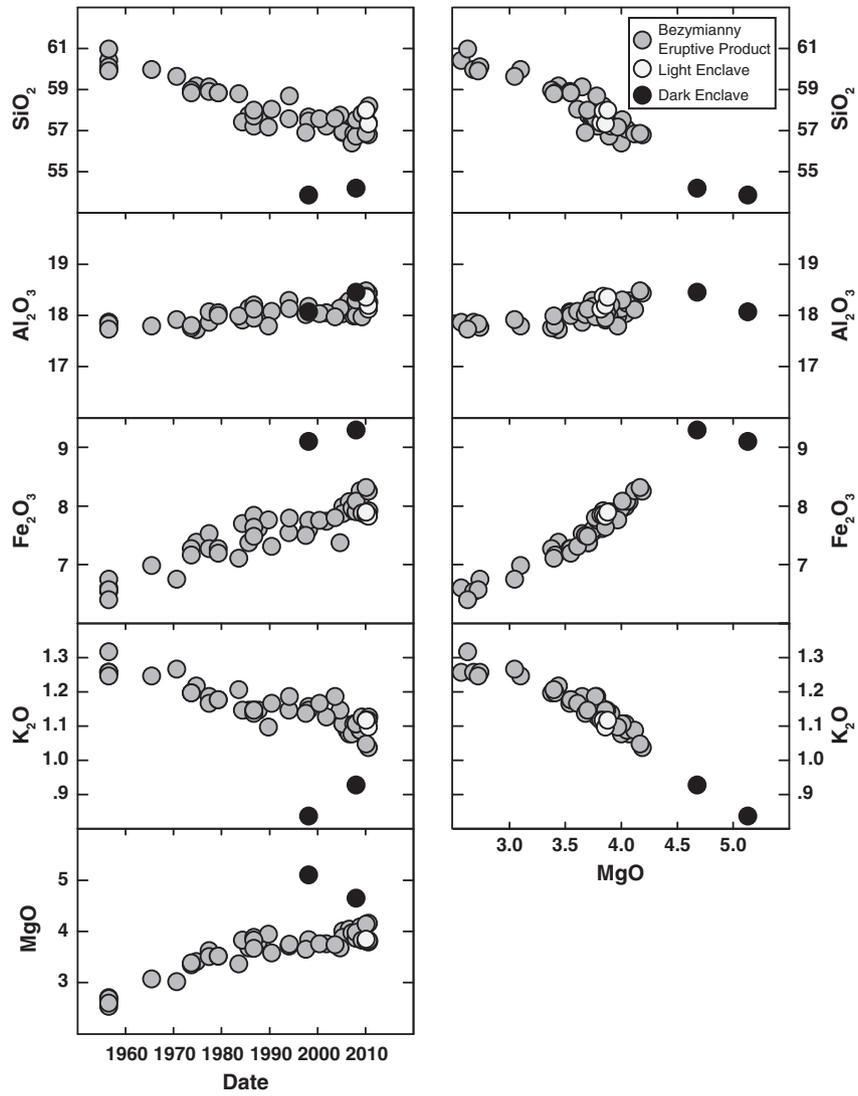
Fig. 1. Whole rock concentrations of Bezymianny eruptive products are andesitic in concentration, and became increasingly mafic between 1956 and 2010.
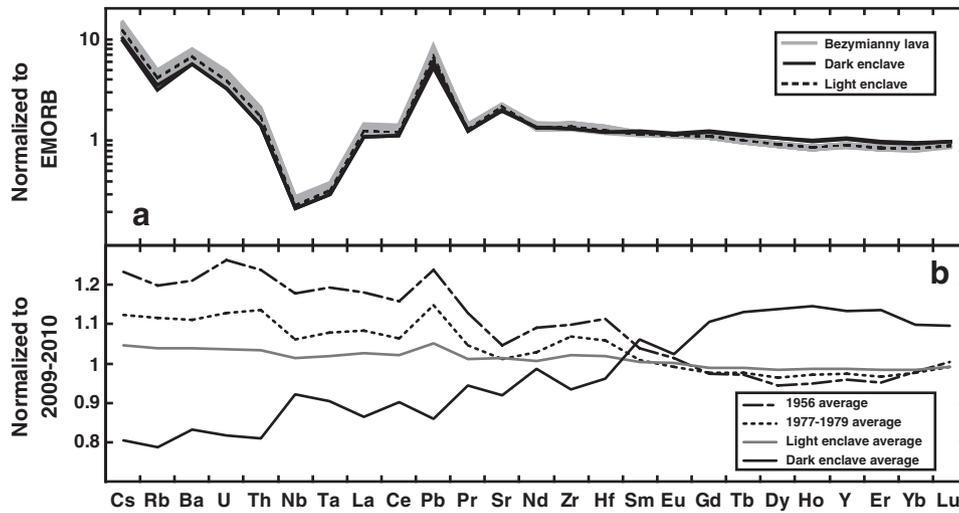

Fig. 2. (a) Spidergram normalized to EMORB (Sun and McDonough, 1989). All samples exhibit characteristic arc lava signatures. (b) Average compositions of samples from 1956 and 1977–1979 as well as average compositions of samples of light and dark enclaves, normalized to the average compositions of samples from 2009 to 2010. Note the increasing abundance of incompatible elements through time, as well as the concave HREE patterns. Note the log scale in the top panel and linear scale in the lower panel, and that the lower panel is normalized to the 2009-2010 composition.

Table 1
Representative whole rock analyses.

Sample	05IPE23a	B-65	B-77	B-1987	BZ1997PF1	10IPE1a	10IPE1b	09IPE67/1
Eruption	1956/3/30	1965/3/10	1977/3/25	1987/6/15	1997/12/5	2010/6/1	2010/6/1	1997/12/5
Material	Bomb	Pyroclastic	Pyroclastic	Lava flow	Pyroclastic	Pyroclastic	Light enclave	Dark enclave
XRF								
SiO_2	60.03	60.02	59.18	57.61	57.72	56.85	57.38	53.92
TiO_2	0.59	0.63	0.71	0.72	0.72	0.80	0.75	0.98
Al_2O_3	17.88	17.81	17.88	17.98	18.20	18.45	18.21	18.09
Fe2O3	6.56	7.00	7.55	7.63	7.62	8.27	7.84	9.12
MnO	0.14	0.14	0.15	0.14	0.14	0.15	0.15	0.14
MgO	2.67	3.09	3.64	3.82	3.74	4.18	3.85	5.12
CaO	6.63	6.85	7.32	7.54	7.52	8.10	7.71	8.21
Na_2O	3.51	3.32	2.99	3.43	3.39	2.89	2.97	2.85
K_2O	1.26	1.25	1.19	1.15	1.16	1.04	1.10	0.84
P_2O_5	0.18	0.18	0.18	0.18	0.18	0.17	0.17	0.16
ICPMS								
TiO_2	0.59	0.62	0.68	0.69	0.71	0.79	0.73	1.00
Na_2O	3.6	3.5	3.5	3.5	3.5	3.5	3.5	3.2
MnO	0.130	0.131	0.135	0.129	0.131	0.140	0.134	0.135
Li	19.4	19.0	18.0	16.9	17.1	15.4	16.9	15.2
Be	0.96	0.92	0.87	0.88	0.84	0.79	0.85	0.73
Sc	13.2	14.8	19.2	19.0	20.0	23.8	21.0	31.8
V	119	138	161	168	174	206	184	278
Cr	13.6	21.2	25.5	20.1	18.9	16.4	16.1	11.1
Co	14.3	16.5	21.6	20.7	22.6	24.1	21.6	31.8
Ni	7.9	10.8	14.1	16.1	15.1	15.6	13.8	22.3
Cu	22.9	32.7	37.7	43.8	44.1	46.1	37.5	210.2
Zn	72.3	74.5	73.9	70.0	71.7	74.8	73.1	80.0
Ga	17.5	17.4	17.1	17.5	17.6	17.6	17.6	17.8
Rb	23.4	23.2	22.2	21.3	21.8	19.2	20.7	16.1
Sr	349	342	335	340	341	332	342	303
Y	19.4	19.2	20.1	19.5	19.6	20.6	20.1	23.3
Zr	109	111	104	102	102	96	100	95
Nb	2.23	2.17	2.00	1.96	1.96	1.83	1.90	1.80
Cs	0.89	0.88	0.82	0.77	0.77	0.69	0.75	0.60
Ba	439	434	407	390	390	351	378	324
La	8.88	8.55	8.32	7.88	7.94	7.39	7.82	6.88
Ce	20.5	19.8	19.2	18.4	18.3	17.3	18.2	16.7
Pr	2.91	2.84	2.78	2.67	2.67	2.57	2.64	2.55
Nd	12.9	12.6	12.6	12.1	12.0	11.8	12.0	12.1
Sm	3.08	3.03	3.04	3.03	3.01	2.97	3.01	3.27
Eu	1.03	1.02	1.03	1.02	1.03	1.02	1.04	1.08
Gd	3.23	3.20	3.33	3.22	3.20	3.34	3.29	3.75
Tb	0.52	0.51	0.53	0.53	0.52	0.54	0.53	0.61
Dy	3.12	3.11	3.26	3.23	3.19	3.36	3.27	3.82
Ho	0.65	0.65	0.67	0.68	0.67	0.69	0.68	0.79
Er	1.89	1.88	1.95	1.94	1.92	2.03	1.98	2.29
Yb	1.97	1.95	2.02	1.97	1.93	2.03	1.99	2.25
Lu	0.32	0.32	0.32	0.31	0.32	0.32	0.31	0.35
Hf	2.78	2.79	2.62	2.60	2.59	2.44	2.55	2.49
Ta	0.18	0.17	0.16	0.15	0.16	0.14	0.15	0.14
Pb	4.63	[a]	4.33	4.01	4.10	3.65	3.85	3.16
Th	1.22	1.20	1.13	1.04	1.07	0.95	1.03	0.87
U	0.85	0.83	0.76	0.74	0.72	0.63	0.69	0.59

[a] Sample B-65 became contaminated in Pb during storage.

4.3. Amphibole thermobarometry and estimates of liquid compositions

The pressure and temperature conditions of amphibole crystallization, as well as the liquid compositions from which the amphiboles likely crystallized, can be calculated from amphibole compositions using the method described in Ridolfi and Renzulli (2012) (hereafter referred to as RR12). We used averaged compositions of transects taken within unaltered amphibole cores for thermobarometric and chemometric calculations. As can be seen in Fig. 7a, thermobarometric results indicate that the amphiboles originated in two distinct zones of pressure and temperature. Zone one falls between 200 and 300 MPa with a temperature of 900 ± 50 °C. Zone two falls between 500 and 750 MPa with a temperature of 975 ± 25 °C. These two ranges of pressure correspond well to the depths of local crustal storage reservoirs of 7 km (Thelen et al., 2010) and 18 km (Fedotov et al., 2010). It should

be noted that following the exact protocol described in RR12 is impractical for the high pressure (high-P) range of compositions, as the pressure range under examination crosses the threshold between two of RR12's recommended equations, creating an artificial discontinuity in the results. Given these circumstances, it is desirable to apply a single barometric method to all of the high-P samples under consideration. The barometric results shown in Fig. 7 are considered optimal for this study, and were calculated as the average of RR12 equations P1b, P1c, and P1e (Filippo Ridolfi, personal communication).

Chemometric results indicate that H_2O contents of the liquids in equilibrium with high-P amphiboles were between 7 and 9 wt.%, while results for low pressure (low-P) amphiboles fall mostly between 4 and 6 wt.% H_2O. As shown on Fig. 7b, the high-P liquids, which are nearly rhyolitic in composition, are undersaturated with respect to H_2O, while the low-P liquid H_2O contents sit very near the
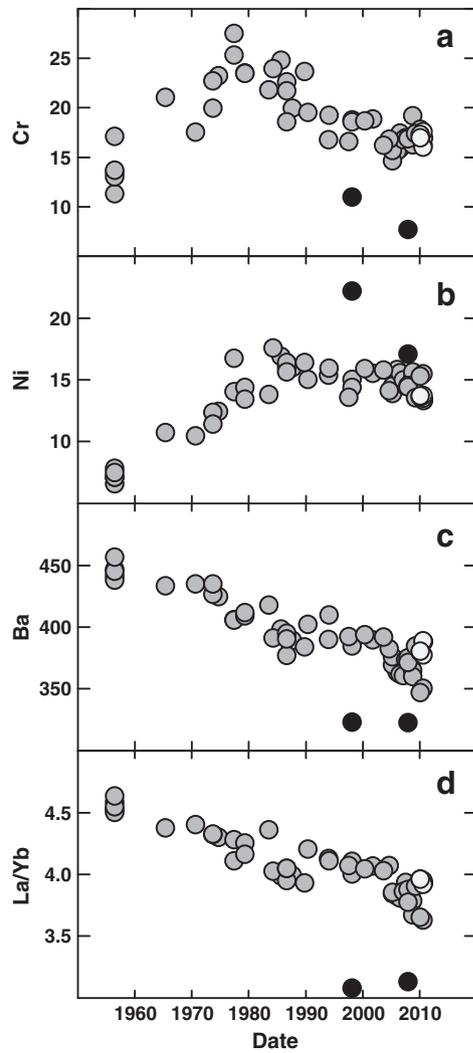
Fig. 3. (a–b) Concentrations of Cr and Ni in Bezymianny eruptive products and enclaves through time. Note the kinks in the late 1970s. (c–d) Concentrations of Ba and the ratio La/Yb decrease from 1956 to 2010.

rhyolitic saturation surface calculated using the VolatileCalc macro of Newman and Lowenstern (2002). Notably, the major element compositions of all liquids (calculated using RR12) are slightly less rhyolitic than the experimental compositions used to calibrate VolatileCalc. As a result, the relevant saturation surface should be shifted slightly away from the rhyolitic curve toward the basaltic curve. The relevant saturation surface for our calculated liquids likely falls within error of the calculated water contents of low-P samples. Therefore, if high-P reservoir liquids (which appear to be mostly H_2O undersaturated) were transferred to the low-P reservoir, they would likely become H_2O saturated and degas significantly during their ascent.

The amphibole-calculated major element compositions of liquids are somewhat more felsic for the low-P group than the high-P group, though both low-P and high-P amphiboles indicate increasingly mafic liquid compositions from 1956 to 2010. This offset between the two groups, combined with the trends toward more mafic compositions within each group, creates parallel trends in plots of liquid composition vs. date (e.g. Fig. 7c). The calculated liquid compositions for the low-P group overlap considerably with and follow the same trend as the compositions of melt inclusions from the outermost rims of plagioclase phenocrysts (Owen Neill & Vasily Shcherbakov, in prep). Calculated liquid Al_2O_3 concentrations are greater in the high-P group, and tend to increase over time within each group, though this increase in Al_2O_3 is larger in the low-P group (Fig. 7d).

5. Discussion

The simplest mechanism capable of producing whole rock compositional variation within a continuously erupting volcano is magma derived from a cooling, homogenous, closed system chamber, where ongoing crystal fractionation will drive the magma toward increasingly felsic compositions. At Bezymianny, however, this is not possible, given that the eruptive products have become increasingly mafic through time (Fig. 1). It follows that the magma system at Bezymianny is either not a closed system, is not homogeneous, or is neither a closed system nor homogenous.

Intermittent eruption of a closed system, compositionally zoned magma chamber, such as those proposed by Hildreth (1983) or Bacon and Druitt (1988), might instead be responsible for the compositional trends at Bezymianny. The simplest compositional variation within a magma chamber is produced by fractional crystallization of a single parent magma prior to the initial eruption. Magma that has undergone a greater amount of fractional crystallization becomes more felsic and decreases in density. The most felsic, least dense, magmas reside at the top of the reservoir, while denser mafic magmas are confined to the bottom. A temporal trend of increasingly mafic products may form as buoyant, felsic magmas are removed from the top of the reservoir by an eruption, leaving deeper, mafic layers of the reservoir to be erupted subsequently (Kadik et al., 1986).

If the compositional variation of a volcano's eruptive products is produced by varying degrees of fractional crystallization, as proposed above, then it will be possible to generate any erupted felsic lava composition by removing some combination of crystallizing phases from any of the more mafic lavas. As can be seen on Fig. 4b, the Cr contents of the Bezymianny eruptive products increase from about 15 ppm to about 30 ppm, a factor of 2, as MgO decreases from 4.2 wt.% to 3.5 wt.%. Over this same range of MgO, highly incompatible elements, such as Th and Cs (Fig. 4e and f), increase by a factor of 1.2. This range of variation is well resolved for all elements given the analytical uncertainties in Electronic Appendix 2. There are no potential crystallizing phases in which Cr has a lower partition coefficient than Th and Cs, therefore these trace element variations could not have been produced via crystal fractionation alone.

Convective self-mixing is another process that has been proposed to create compositional diversity among mineral populations, and potentially among whole rock compositions, within a single magma chamber that is heated from below and cooled from above (e.g. Couch et al., 2001; Ridolfi et al., 2008). Magma at different temperatures will crystallize minerals of different compositions, with cooler portions of the magma chamber crystallizing to greater degrees. If contrasting mineral and liquid populations are then partially remixed by convection within the magma chamber, a range of whole rock compositions could be produced. It is unclear, however, how such a process could produce the trend toward increasingly mafic whole rock compositions over the course of 54 years of activity at Bezymianny. Furthermore, plagioclase textures and compositional zoning patterns in Bezymianny eruptive products appear to rule out convective self-mixing in favor of conventional magma mixing (Shcherbakov et al., 2011). Mixing between two magma bodies would have resulted in a perfectly linear array on Fig. 4a–b, and a nearly linear array on Fig. 4c. Because the compositional arrays on both of these diagrams are kinked, a simple mixing model between two compositional end members is also not consistent with the data.

5.1. A three component mixing model for Bezymianny

A three component magma mixing system can account for the compositional arrays seen in the eruptive products of Bezymianny. As noted earlier, such a mixing model requires an abrupt change in mixing components around 1977 in order to account for the shifts in trajectories seen in Fig. 3a and b. It is likely that the 1977 kink is
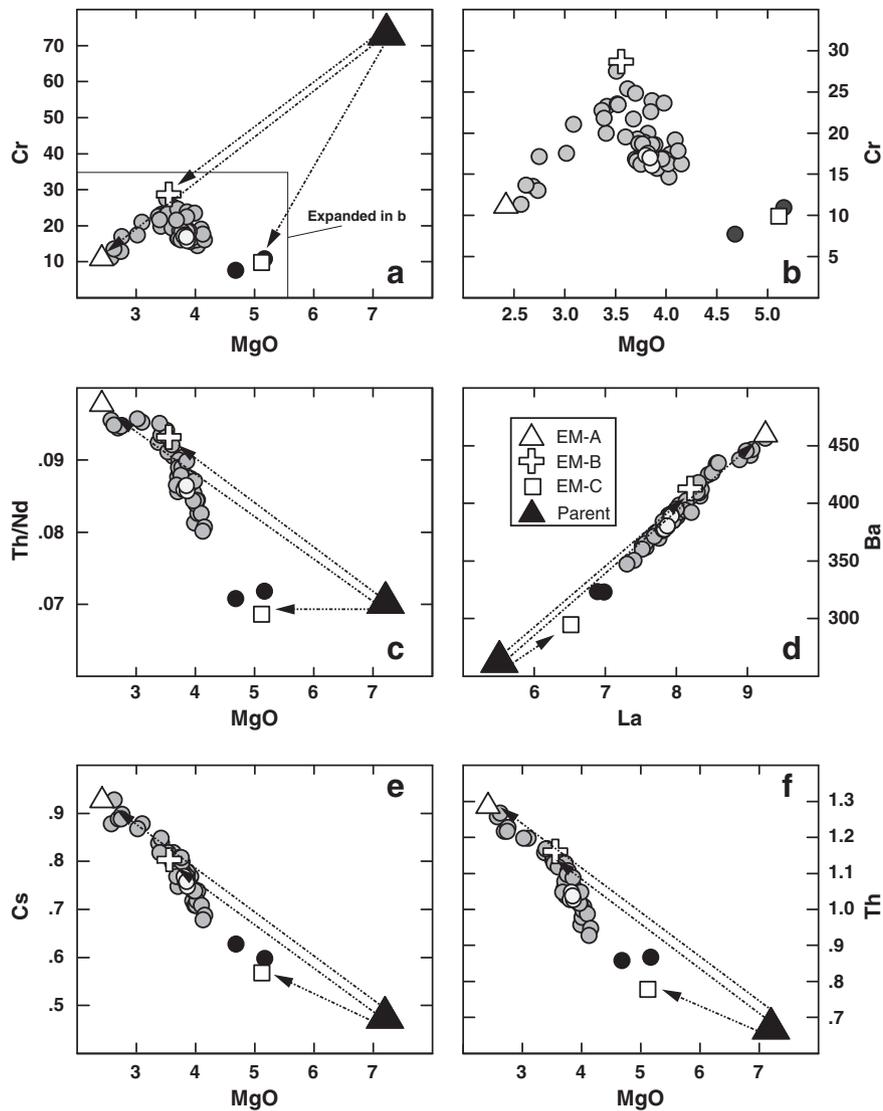
Fig. 4. (a–c) Plots of Cr and Th/Nd vs MgO produce kinked arrays, which cannot be produced by simple fractional crystallization or two component mixing. The arrays can be reproduced by three component mixing between the end-members EM-A, EM-B, and EM-C. These end-members can be modeled as the products of fractional crystallization of a single parental composition via the removal of different mineral assemblages, presumably caused by fractionation at varying pressures. Lines with arrows show fractional crystallization paths discussed in text. (d) On this plot of Ba vs La, as well as many other element–element plots, the sample compositions form simple linear arrays.

a result of either the addition or removal of a mixing component at this point in time. For a straightforward three component mixing model, two of the components are fairly well constrained on the plot of Cr vs MgO (Fig. 4b). As shown on Fig. 4b, the samples with both the highest and lowest MgO concentrations have 10 ppm Cr or lower, while samples with intermediate MgO contents trend toward higher Cr. In order to encompass the entire range of compositions on Fig. 4b, one of the mixing components must have low MgO (<~2.5 wt.% MgO) and low Cr, while another must have >~5 wt.% MgO with similarly low Cr. If two out of three mixing components have low Cr concentrations, then the third mixing component must have higher Cr concentrations. Qualitatively, three component mixing appears to be a plausible mechanism for producing the compositional diversity of the eruptive products of Bezymianny. A quantitative evaluation is presented in Section 5.2.

Amphibole themobarometry and chemometry results are also consistent with a three component mixing model for Bezymianny. As discussed above, amphibole crystallization appears to have occurred in two distinct zones of pressure and temperature, which presumably correspond to two distinct magma reservoirs. In some cases, amphiboles from each of the two regions appear in a single sample, which indicates that the whole rock assemblages are produced via mixing between magmas derived from at least two reservoirs. Also, as shown in Fig. 6, in some cases the high Al_2O_3, high pressure amphibole compositions are surrounded by low Al_2O_3 rims, indicating that the individual amphibole crystal initially crystallized in the high-P reservoir, and was later transferred to the low-P reservoir, where it continued to grow. The offsets in calculated liquid compositional trends (Fig. 7c and d) indicate that two reservoirs contain liquids with unique compositions, and that the liquid compositions of each reservoir individually become more mafic over time.

The offset in liquid compositions could result from either different whole rock compositions in the reservoirs, or different proportions of crystallized minerals and liquids. The trends toward increasingly mafic compositions over time indicate that each reservoir was injected with a continuous input of a liquid that was more mafic than the initial liquid composition of that reservoir. The composition of the low pressure reservoir was likely modified by injection of liquid from the high pressure reservoir, causing the low-P liquids to become more similar to the initial high-P liquids over the course of the eruptive cycle. The high-P reservoir also became more mafic, however, indicating that it was injected with a third, even more mafic liquid. This
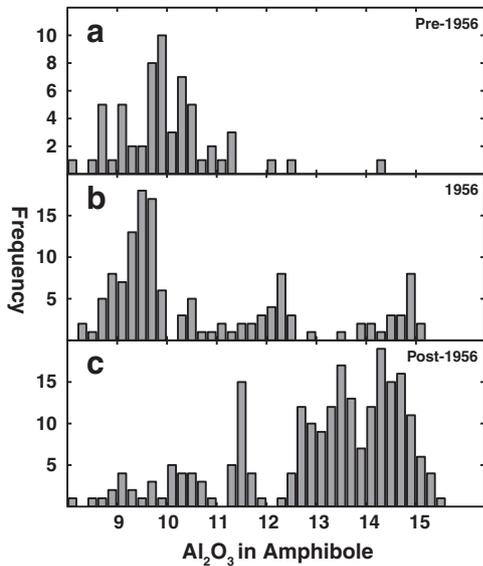
Fig. 5. The concentration of Al_2O_3 in amphibole phenocrysts forms a bimodal distribution. (a) In the pre-climatic ash, Al_2O_3 content is unimodal and ranges from 8 to 12.4 wt.% (b) Amphiboles from the climactic eruption show wider compositional variations with Al_2O_3 content as high as 14–15 wt.%. (c) Though rare, amphiboles erupted after 1956 cluster around 13 to 15 wt.% Al_2O_3.

third, most mafic, liquid is presumably derived from a third reservoir which did not itself contribute amphiboles to the erupted material.

5.2. Solving for mixing end-members

In order to quantitatively assess whether a three end-member mixing model can account for the complete range of compositions, end-member-mixing-analysis was undertaken, following Weltje (1997). This method is preferable to standard principle component analysis or factor analysis because it ensures that each measurement of the individual samples can be reproduced within error from nonnegative end-members and mixing proportions. Elements that became contaminated during storage in multiple samples (Zn, Pb) and elements for which measured compositions for some samples approached analytical limits (Co, Ni, Cu) were not included in the mixing analysis.

End-member-mixing-analysis consists of two main stages. First, a linear approximation of the composition matrix (the set of elemental compositions measured in each sample) must be constructed based on an assumed number of components. In this stage, the compositions of all elements can be scaled following a variety of different methods (Miesch, 1980). For our model it is desirable for the linear approximation of the data to be close to the actual measured data

on average. However, it is also desirable to minimize the maximum discrepancy between any measurement and its associated approximation. In order to meet these goals, scaling coefficients were selected by a weighted least squares minimization of both the average difference and maximum single difference between the actual and approximated data.

If the dark enclaves are not included in the model, the maximum difference between any observation and its model approximation is 6%, with an average difference of only 1.2%. For major and minor elements, the maximum differences are 4.6% and 4.2% and the average differences are 0.8% and 1.4%. If the dark enclave 09IPE65b is included in the model, the maximum and average differences between the model and measured trace elements are 8% and 1.4% (direct comparison in Fig. 8). For major and minor elements, the maximum differences are 5.1% and 7.4% with average differences of 0.9% and 1.5%. The discrepancies between the model output and actual measurements are small considering the analytical uncertainty and heterogeneity within sampled material likely to exist in a natural system.

5.3. Temporal variation in end-member mixing proportions

Once the approximated composition matrix has been calculated, it is possible to solve for end-member compositions. The end-member compositions are whole rock values, since the aim is to account for the total lava compositions. A weighted least squares procedure was used to obtain nonnegative end-member compositions and the corresponding nonnegative mixing proportions for each sample that perfectly reproduced the approximated composition matrix. As outlined in Weltje (1997), the algorithm searches for a scaled loading matrix that, in combination with the approximated composition matrix and its associated reference vectors described in the previous section, can be used to compute end-member compositions that are non-negative and a set of mixing proportions that are both non-negative and sum to one for each sample. Our procedure utilizes MATLAB's active-set algorithm rather than the specific iterative algorithm described by Weltje (1997), though improvements in processing power enable quick calculations using either method.

As discussed in Section 5.1, the compositions of two of the mixing end-members (EM-A and EM-C) are fairly well constrained. Best-fit solutions for these end-members are similar to the compositions of the 1956 lavas and the mafic enclaves. Any end-member solutions that are more distant from the compositions of the 1956 lavas and enclaves will either approach negative Cr concentrations or produce mixing proportions that do not sum exactly to one. The third mixing end-member (EM-B) can be assigned a range of compositions constrained to a compositional vector that is roughly defined by a line connecting the compositions of the 1956 and 1977 eruptives. The minimum MgO contents of EM-B are similar to those of the eruptive
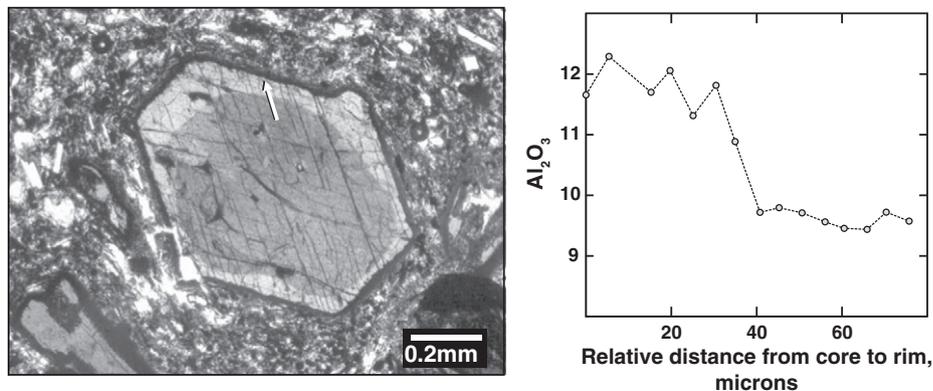

Fig. 6. Photomicrograph showing amphibole phenocrysts with high-Al core and low-Al rim from the Bezymianny andesite erupted on March 30, 1956. The white arrow indicates the location of the electron microprobe profile shown on the right.
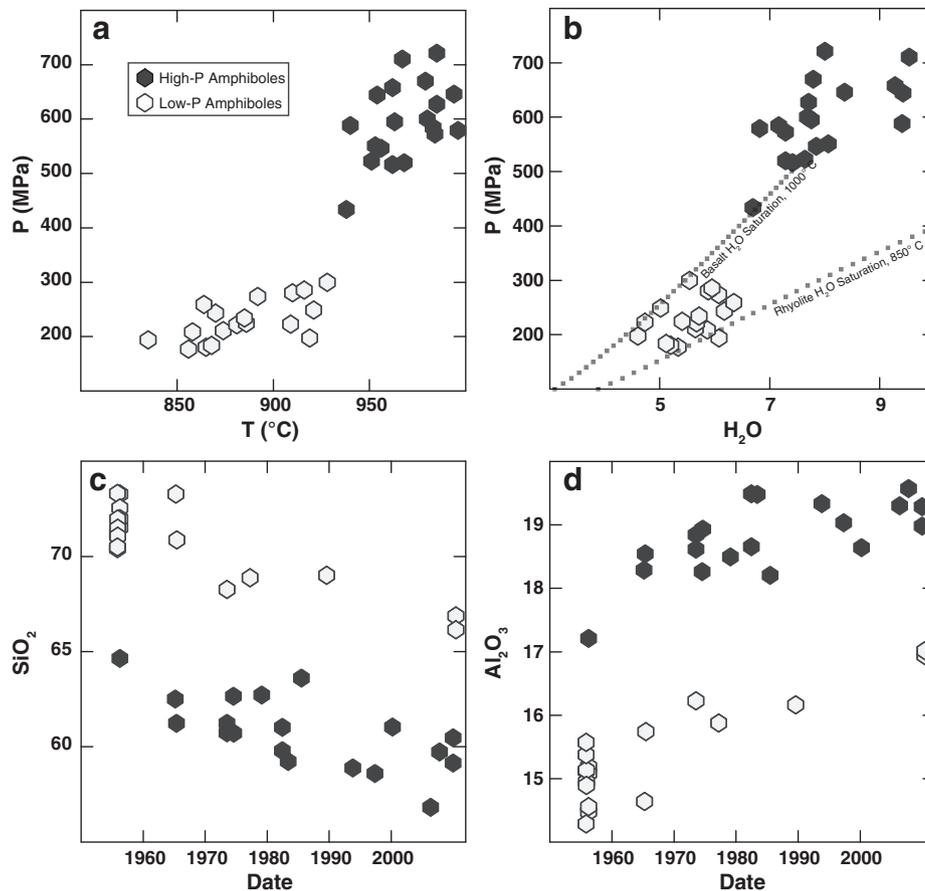
Fig. 7. Results of amphibole thermometric, barometric, and chemometric equations from Ridolfi and Renzulli (2012). (a) The amphiboles reflect equilibration temperatures from two distinct zones in P and T space. (b) The high-P amphiboles are in equilibrium with a liquid that is >7% H₂O, while the low-P amphiboles reflect liquids of <7%. The H₂O saturation lines were calculated with VolatileCalc, using default Rhyolite composition and a basalt with 49% SiO₂. As the high-P liquids are transferred to the low-P reservoir, the liquids most likely cross their H₂O saturation surface and degas significantly. (c) Amphibole concentrations reflect more mafic liquids in the high-P chamber than in the low-P chamber. Both liquids become increasingly mafic from the onset of volcanic activity to present day. (d) The low-P liquids are offset to lower concentrations of Al₂O₃. This is likely due to a greater degree of plagioclase fractionation from the low-P liquids, which also have lower concentrations of H₂O.

products of 1977. The maximum MgO is not constrained mathematically, but if higher MgO is assigned to EM-B, larger proportions of EM-A are necessary to produce the 1977 compositions. Varying MgO in EM-B causes the proportions of mixing end-members with time to vary, and determines whether EM-A can go to near zero after 1977. Two possible solutions, to be discussed further in the following section, are presented in Electronic Appendix 4.

In Scenario One, EM-B is as similar as possible to the eruptive products of 1977. Fig. 9 shows how the three end-members would then vary between 1956 and 2010. The volcano begins to erupt in 1956 with a composition of almost pure EM-A. The proportion of EM-A decreases continuously between 1956 and 1977, possibly undergoing a minor resurgence in the 1990s. By 1977, EM-A contributes negligibly

to the erupted material (considering model error and the constraint that mixing proportions be >0), at which point EM-B begins to dominate erupted compositions. EM-C, the most mafic end-member, first appears significantly in 1977, reaching over 50% in 2010.

In Scenario Two, EM-B is calculated assuming 5 wt.% MgO (as opposed to 3.56 wt.% in Scenario One). As in Scenario One, the initial composition is almost entirely EM-A. As of 1977, the proportion of EM-A levels off to about 50% of the erupted material, with EM-B contributing the other 50%. If EM-B had still higher MgO concentrations, the maximum contributed proportion of EM-B would be still lower, and the minimum contribution of EM-A still higher. EM-C increases progressively in significance after 1977. Therefore, the key difference in the two scenarios is whether EM-A becomes negligible after
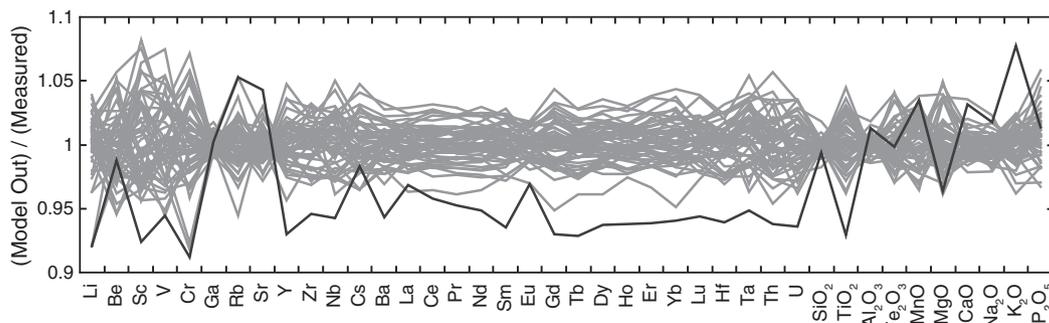

Fig. 8. Comparison between measured whole rock compositions and mixing model results. Each of the gray solid lines shows the difference between the measured and modeled composition for an individual sample. The dark solid line shows the difference between measured and modeled composition for the mafic enclave.
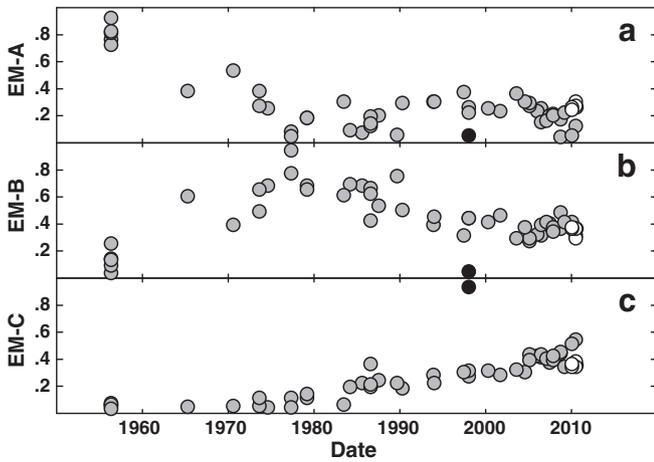
Fig. 9. Mixing proportions of the three calculated mixing end-members for each sample from 1956 to 2010. These mixing proportions are for model Scenario One. In Scenario Two, EM-A only decreases to 0.5 by 1977, after which it remains fairly level. Plots for Scenario Two are available in Electronic Appendix 4.

1977, or continues as an important mixing end-member. In Scenario Two, all three mixing end-members contribute significantly to the eruptive products following 1977, while in Scenario One, the eruptive products after 1977 are primarily a mixture of EM-B and EM-C.

While the details of the end-member analysis are non-unique, we prefer Scenario One. First, this scenario uses end-members that correspond with erupted compositions, rather than inferring an alternative end-member for which there is no independent evidence. Second, there are sound mineralogical arguments that EM-A becomes negligible after 1977. As discussed previously, low aluminum, low pressure amphiboles dominate the phenocryst population of the eruptive products from 1956 to 1965, but are rare in all material erupted since that time. It is logical that these low pressure amphiboles are a component of EM-A, which dominates the eruptive products of 1956. The scarcity of low pressure amphiboles in later eruptions suggests that the proportion of EM-A in erupted material most likely diminished rapidly after the initial eruptions. This petrologic constraint favors Scenario One over Scenario Two, because Scenario Two requires that significant contributions from EM-A persisted from 1956 up to 2010. Model results from Scenario One will for this reason be the basis for the discussion in the following section.

5.4. Origin of the diversity of end-member compositions

It is worth considering whether the three end-member compositions might be related by isobaric fractionation from a common parental magma, along a single liquid line of descent (LLD). The possibility that the end-member compositions are produced by a single fractionation sequence can be ruled out, however, for the same reason that this relationship was discounted within the individual samples. As shown in Fig. 4b, if the mixing end-members were related by a LLD, the Cr contents must have increased from about 10 ppm to about 30 ppm between EM-C and EM-B, a factor of 3. The highly incompatible elements Th and Cs, however, increase by less than a factor of 2 during this same interval. As stated earlier, there are no potential crystallizing phases in which Cr has a lower partition coefficient than Th or Cs, therefore these trace element variations could not have been produced via crystal fractionation alone.

Though the end-members are not related by a single LLD, it is still possible that the end-member compositions evolved from a common parental magma through fractional crystallization of distinct mineral assemblages owing to differences in pressure and associated volatile content. To quantitatively assess the possibility of a single parental magma composition, a least squares model has been constructed that

incorporates our end-member whole rock compositions and amphibole analyses, the pyroxene and plagioclase analyses of Shcherbakov et al. (2011), Fe–Ti–Oxide analyses (Jill Shipman, unpublished data), as well as partition coefficients for each of these phases (from multiple sources, see Electronic Appendix 4). This model uses the equation for bulk fractional crystallization, operating under the assumption that the pure mixing end-members approximate the compositions of liquids fractionated from a single mafic parent. Though the material erupted at Bezymianny contains varying quantities of phenocrysts, the material is texturally and compositionally homogenous, with glass and mineral compositions that generally track the bulk rock compositions (Jill Shipman, personal communication). The model found a single parental composition that could be fractionated to produce each of the end-members to within 2.6% for major elements (4.5% for K_2O), with an average difference of 1.4%, and to within 8.1% for trace elements, with an average difference of 3.4%. This parental composition (Table 2) is fractionated 49% to obtain EM-A, 41% for EM-B and 17% for EM-C. The calculated parental magma is a high-Mg basalt, and is similar to some of the eruptive products of Kliuchevskoi volcano — Bezymianny's massive neighbor 10 km to the north. Fractionating assemblages used in the model are reported in Table 3, and detailed model results as well as a comparison to Kliuchevskoi can be found in Electronic Appendix 4.

EM-A and EM-B have similar fractionating assemblages, though EM-A was set to form via fractionation of a lower pressure (lower Al_2O_3) amphibole composition. This constraint was imposed because,

Table 2
Calculated mixing end-member and parental magma[*] compositions for Scenario One, as discussed in the text.

	EM-A	EM-B	EM-C	Parent
SiO_2	60.90	58.34	53.17	51.86
TiO_2	0.56	0.65	0.95	0.93
Al_2O_3	17.83	17.79	18.38	16.84
Fe_2O_3	6.35	7.27	9.29	10.27
MnO	0.13	0.13	0.14	
MgO	2.42	3.56	5.10	7.20
CaO	6.45	7.26	8.60	8.54
Na_2O	3.72	3.48	3.23	2.69
K_2O	1.32	1.20	0.88	0.76
P_2O_5	0.19	0.18	0.16	
Li	20.51	17.78	13.52	
Be	0.97	0.88	0.70	
Sc	11.42	17.71	30.50	36.80
V	103	153	272	
Cr	11.29	28.66	10.01	73.63
Ga	17.61	17.23	17.81	
Rb	24.95	22.72	16.39	14.84
Sr	354	340	313	268
Y	19.21	19.04	21.78	
Zr	110.4	105.8	88.9	72.09
Nb	2.27	2.01	1.66	
Cs	0.93	0.82	0.57	0.48
Ba	460	412	295	266
La	9.26	8.20	6.49	5.51
Ce	21.16	18.89	15.61	13.19
Pr	3.01	2.71	2.39	
Nd	13.17	12.13	11.35	9.62
Sm	3.10	2.97	3.05	2.66
Eu	1.05	1.00	1.05	0.95
Gd	3.21	3.13	3.50	
Tb	0.51	0.51	0.57	0.48
Dy	3.08	3.10	3.61	
Ho	0.64	0.65	0.75	
Er	1.87	1.87	2.16	
Yb	1.96	1.91	2.12	1.76
Lu	0.32	0.31	0.33	0.28
Hf	2.83	2.65	2.30	1.81
Ta	0.18	0.16	0.13	0.11
Th	1.29	1.13	0.78	0.68
U	0.88	0.77	0.53	

[*] Missing parent magma values are due to lack of reliable partition coefficients for all phases.

Table 3
Mineral assemblages and proportions used in fractionation model.

	EM-A	EM-B	EM-C
	Total fractionation		
	49%	41%	17%
	% Fractionating proportions		
Ol	20	18	0
Plag1	31	33	9
Plag2	6	0	0
Cpx	3	0	43
Opx	0	0	46
Hbl1	35	0	0
Hbl2	0	44	0
Mt	5	6	0
Il	0	0	1

as indicated above, the lower Al_2O_3 amphiboles are far more prevalent in samples from 1956, which are dominated by EM-A. The fractionating assemblages determined for EM-A and EM-B are roughly consistent with the experimental results of Grove et al. (2003) at the two P and T conditions calculated from amphibole thermobarometry.

EM-C is marked by the lack of amphibole in the crystallizing assemblage. The high percentage of pyroxenes, and lack of amphibole, in the assemblage for EM-C may be possible at pressures of greater than 1000 MPa, outside of the zone of amphibole stability. Though experimental verification under these crystallizing conditions has not been carried out for the exact compositions in question, experimental results for liquid compositions that are similar to the proposed Bezymianny parental composition support this fractionation model (Gust and Perfit, 1987; Liu et al., 2000). Additional support for crystallization of a pyroxene rich, amphibole free assemblage at high pressures is provided by the work of Shcherbakov and Plechov (2010), who examined crystallizing veins of volcanic glass exhumed in the extremely rare mantle xenoliths that were erupted at Bezymianny in 2007.

A zone of high pressure fractionation above the amphibole stability limit is also consistent with local seismic observations of a thickened crust (up to 42 km) in the region surrounding Bezymianny, likely due to extensive basaltic underplating (Balesta, 1991; Churikova et al., 2001). Alternatively, high pressure crystal fractionation could have been generated within the region of deep magma storage recently proposed by Koulakov et al. (2011) using seismic tomography.

A final test of both the mixing and fractionation models can be performed by considering the model results along with the liquid compositions calculated from amphiboles. If the results of the fractionation model are valid, then it should be possible to reproduce the mixing end-members, which represent whole rock compositions, by taking phenocrysts that are similar to the fractionating assemblages and adding liquids to them. The liquid compositions calculated via the chemometric amphibole equations of RR12 then provide an opportunity to test both the mixing and fractionation models simultaneously.

As mentioned previously, the low pressure amphiboles, which were far more abundant in the earlier eruptions, are likely to be a component of EM-A, therefore these low-P amphiboles provide appropriate estimated liquid compositions for this end-member. EM-B is the only other mixing end-member that requires amphibole crystallization, suggesting that the high pressure amphiboles are a component of EM-B. The earliest sample with multiple high pressure amphiboles is sample B-65, a juvenile clast of a pyroclastic flow erupted in 1965. We use these amphiboles to estimate the high pressure liquid composition.

Using least squares optimization, we were able to find a range of possible combinations of mineral assemblages that are both consistent with the fractionation model and can be combined with the liquid compositions (calculated using RR12) to reproduce the whole rock compositions of EM-B and EM-A (major elements fit within 1%,

TiO_2 and K_2O fit within 9%). The best fit solution can be found in Electronic Appendix 4. The data in this study thus are consistent with a model in which independent mixing end-members are produced from a common parental magma by crystal fractionation at different pressures. Though the mixing end-members may have a more complicated origin, the petrological data and analysis do not require it.

5.5. Physical model

A physical model of the Bezymianny magma system consistent with the above analysis must provide a mechanism for the storage and crystal fractionation of a single parental magma at three discrete pressures. Magmas stored at each of these pressures mix together in various proportions to form the erupted compositions of Bezymianny lavas. Following the end-member-mixing-analysis, the earliest episodes of the current eruptive cycle primarily tapped the lowest pressure reservoir (RES-1), which is at a pressure of 200 to 300 MPa, and which initially held magma similar in composition to EM-A. Between 1956 and 1977 the eruptive products became increasingly dominated by EM-B magma, which had been stored at a somewhat higher pressure (500 to 750 MPa) in a second, deeper reservoir (RES-2). Starting in 1977 EM-C magma (the end-member produced by the lowest amount of fractionation at the highest pressure), began to mix into the erupted magmas. By 2010 EM-C accounted for ~56% of the total erupted composition. This constant influx of mafic magma is consistent with the results of Shcherbakov et al. (2011), who found evidence for frequent mafic recharge of the Bezymianny system between 2000 and 2007 on the basis of plagioclase zoning.

As shown in Fig. 10, it is likely that RES-1 and RES-2 are connected in series. The trends toward increasingly mafic liquid compositions within each of these reservoirs, demonstrated using the chemometric amphibole equations of RR12 (Fig. 7c), show that both RES-1 and RES-2 are continuously replenished by mafic magma beginning soon after the onset of the eruptive cycle. The results of end-member mixing analysis show that the magma initially contained in RES-1 is injected with magma from RES-2, while RES-2 is apparently replenished by mafic magma (EM-C), from depth. Only RES-1 is directly connected to the vent, and so the erupted composition at the beginning of the current eruptive cycle is dominated by EM-A. Between 1956 and 1977, the EM-A magma in RES-1 erupted and was then gradually diluted by EM-B magma, drawn from RES-2. The EM-C laden magma was then drawn upward, toward RES-1, and erupted.

5.6. Comparison to Mount St. Helens and Soufrière Hills

Bezymianny volcano has been compared to Mount St. Helens (MSH) in terms of seismicity, eruptive dynamics, deposits, and petrology (Belousov et al., 2007; Thelen et al., 2010). However, the physical model of Bezymianny's plumbing system described above differs significantly from the detailed (Pallister et al., 1992, 2008) models of MSH. During the 1980–1986 eruption of MSH, the erupted material was initially composed of 64–65% SiO_2. As the eruption proceeded, wt.% SiO_2 in the MSH lava decreased, reaching 61% by the middle of 1981. At this point, SiO_2 concentrations began to rise, and by 1986 had rebounded back to 64%. The magmas from the entire 1980–1986 episode were drawn from a depth of about 8.6 km. The 2004–2006 MSH eruptive products had a constant SiO_2 concentration of about 65%, and were drawn from a depth of about 5.2 km.

The magma system at MSH is modeled as a large, compositionally stratified reservoir; the compositional variations in this model are essentially a result of the reservoir being tapped at varying depths. Pallister et al. (1992) demonstrate that the shift toward more mafic magmas in 1981 can be produced as the fluid dynamic result of prior magma withdrawal. The deeper, less silicic magma is drawn into the conduit as the overlying dacitic magma is erupted. As the eruption slows down, the more buoyant dacitic magma once again dominates
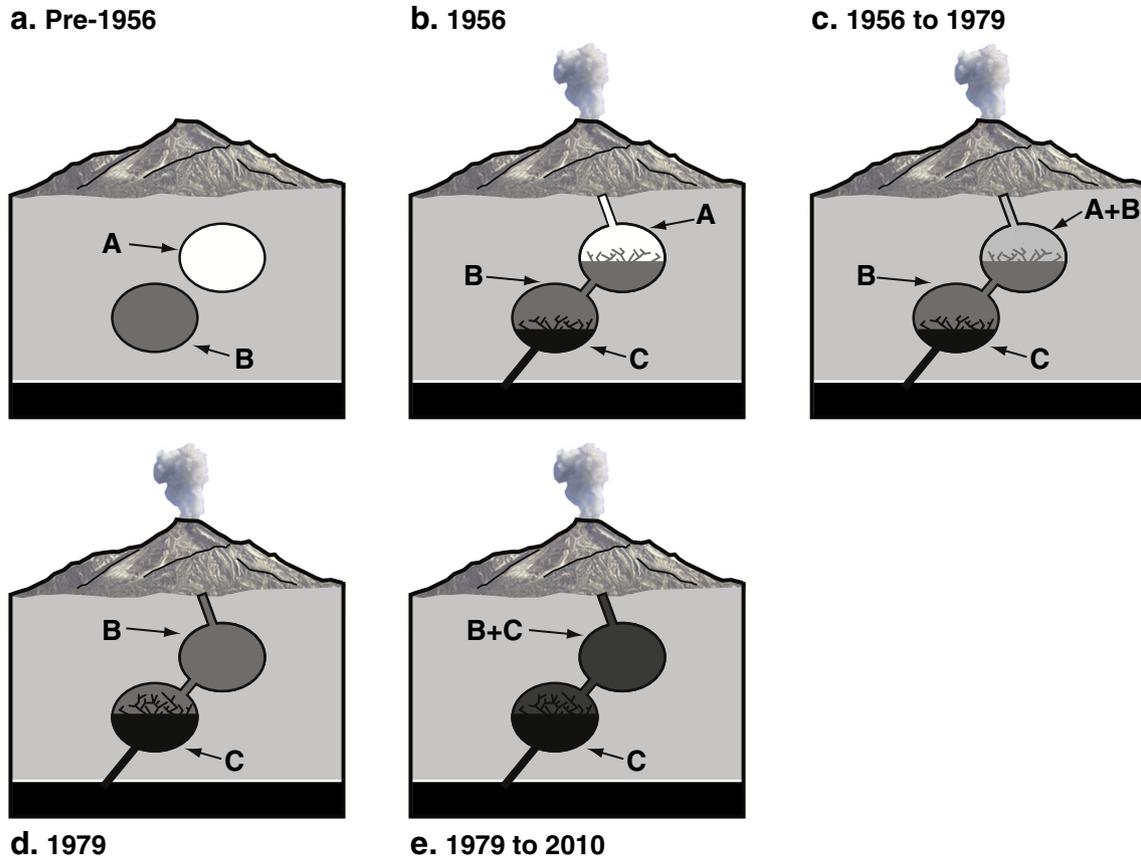
Fig. 10. A cartoon model of physical processes capable of reproducing the model findings of this study. (a) Prior to 1956, the three mixing components of Bezymianny evolved in isolation, via crystal fractionation of a common source. (b) In 1956, influx of mafic magma into the lower chamber triggers an eruption. The 1956 eruption samples primarily the original composition of the upper magma chamber. (c) Between 1956 and 1979, the EM-A magma that originally dominated the upper chamber becomes increasingly diluted by EM-B magma, which originally filled the lower chamber. (d) By 1979, influence of EM-A magma has become very minor. Compositions of erupted magmas in the late 70s are primarily composed of EM-B. (e) Between 1979 and 2010, the erupted compositions become increasingly dominated by EM-C.

erupted compositions. The compositional variations in the 1980–1986 MSH lavas appear to be consistent with two-component mixing. The 2004–2006 eruption produced magmas with compositions that do not lie along the 1980–1986 trend, and are best accounted for as a separate batch of magma that pooled just beneath the roof the reservoir (Pallister et al., 2008).

Soufrière Hills volcano (SHV), which is also similar to Bezymianny in terms of recent activity and eruptive dynamics (Belousov et al., 2007), may resemble it much more closely in terms of its underlying

magma system than MSH. While the bimodal pressure distribution derived from the amphibole compositions of Bezymianny lavas is not seen at MSH, it has been observed within the amphiboles of SHV (Fig. 11, adapted from Fig. 6 of Ridolfi et al., 2010). At SHV, the existence of two discrete reservoirs within the crust has also been independently proposed on the basis of magma efflux and surface deformation, with crustal chambers at 6 km and 12 km below the surface (Elsworth et al., 2008). Though the crisp temporal trends in bulk erupted lava compositions at Bezymianny are not present at
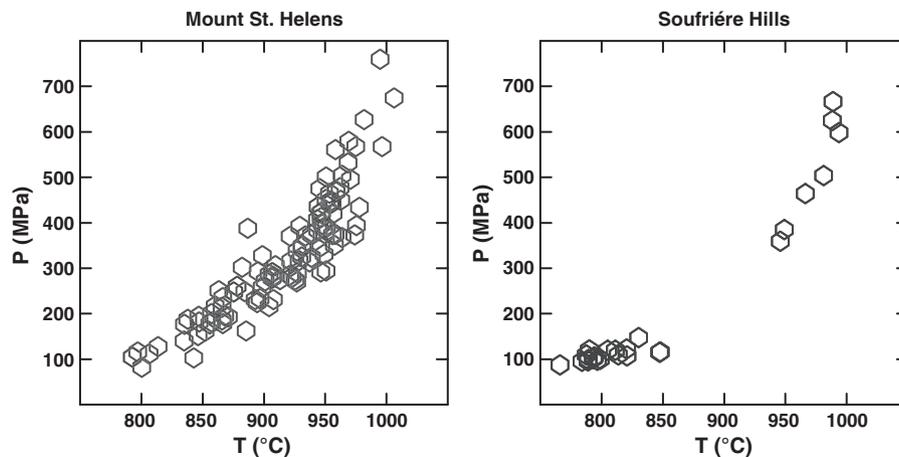

Fig. 11. Pressure and temperature ranges in equilibrium with amphiboles from Mount St. Helens and Soufrière Hills. Figure adapted from Fig. 6 of Ridolfi et al. (2010), using the thermobarometric equations from that study.

SHV, the lavas at SHV are not well homogenized, and contain abundant mafic enclaves (Zellmer et al., 2003). Barclay et al. (2010) noted that the number of mafic enclaves at SHV has increased significantly between 1997 and 2007; thus, on a broader scale, the bulk erupted composition of SHV magmas is also becoming systematically more mafic with time. For these reasons, while the MSH system appears to be quite different from that of Bezymianny, SHV may be an excellent analog. Both the chemical trends examined in this study, as well as Shcherbakov et al. (2011)'s study of plagioclase phenocryst zoning, strongly suggest that the Bezymianny system is undergoing recharge by mafic magma from depth. This contrasts with MSH, where there is no chemical evidence requiring models to incorporate recent emplacement of mafic magma.

It is worth considering what factors may trigger episodes of mafic recharge, which are generally associated with large-amplitude eruptive cycles. The 1980 eruption at MSH was triggered by rapid unloading of pressure owing to a large earthquake-generated-landslide, rather than an influx of mafic magma from below (Pallister et al., 1992). Though the current activity at MSH does not appear to be actively driven by mafic recharge, there is evidence for recharge at MSH during the earlier Kalama eruptive period, which started in 1480 and lasted about 300 years (Pallister et al., 1992). While it is certainly the case that the emplacement of mafic magma can initiate an eruptive cycle (e.g. Pinatubo, 1991, according to Pallister et al., 1996), it is also conceivable that an eruptive cycle triggered by a mechanism similar to the 1980 MSH eruption could itself lead to a new episode of mafic recharge. Such an eruptive episode, though not characterized by an initial influx of mafic magma, could result in significant unloading of the underlying system as the volcano erupts, which may in turn cause new magma to be drawn up from depth. The onset of the current eruptive cycle at Bezymianny is illustrated in Fig. 10 as the result of mafic recharge, though Bezymianny's deep mafic component (EM-C) does not appear to have contributed significantly to bulk rock compositions until at least 22 years after the volcano reawakened (Fig. 9c). From our data, it is not possible to determine whether the initial eruptions of the current eruptive cycle were driven by mafic recharge, or the mafic component began to infiltrate the lower chamber as a result of the initial eruptions. Collaborative work combining thorough seismic, geodetic, and chemical datasets for individual volcanoes through time may provide some resolution of such questions in the future.

6. Conclusions

This study provides constraints from bulk rock trace element and amphibole major element concentrations on the magma supply system of Bezymianny volcano. Our findings can be summarized as follows:

(1) The eruptive products of Bezymianny became increasingly mafic from 1956 to 2010. The major and trace element variations of Bezymianny eruptive products require that chemical variability during this interval was caused by magma mixing.
(2) Major element compositions of Bezymianny amphiboles have a bimodal distribution, which likely correspond to crystallization in two discrete reservoirs, with one between 200 and 300 MPa and another between 500 and 750 MPa. This suggests that the Bezymianny mixing components were initially stored in separate reservoirs, rather than a single compositionally zoned reservoir.
(3) Kinks in the arrays of several trace element plots, together with end-member-mixing-analysis, demonstrate that a total of three mixing components are both necessary and sufficient to account for the bulk compositions of all Bezymianny eruptive products, as well as the majority of enclaves.
(4) The compositions of the three mixing components, determined via end-member-mixing-analysis, can be produced from a common parental magma. If end-member magma compositions

were produced from a common parental magma, it must be the case that each was produced via a unique fractionating mineral assemblage. These unique mineral assemblages are likely caused by different pressures of crystal fractionation.
(5) The constraints listed above can be combined to infer a physical model of the Bezymianny system from 1956 to 2010. Though Bezymianny is in many regards very similar to MSH, the physical model proposed in this work differs in several important ways from models of MSH, while models of SHV are much better analogs.

The model proposed can be tested by experimental studies under the appropriate conditions. Isotopic studies could be used to test whether the magmas of the current eruptive cycle were derived from a common parent, and U-series data could test or constrain the proposed timing.

Supplementary data to this article can be found online at http://dx.doi.org/10.1016/j.jvolgeores.2012.12.014.

References

Al'meev, R., Ariskin, A., Ozerov, A., Kononkova, N., 2002. Problems of the stoichiometry and thermobarometry of magmatic amphiboles: an example of hornblende from the andesites of Bezymyannyi Volcano, Eastern Kamchatka. Geochemistry International 40, 723–738.

Bacon, C.R., Druitt, T.H., 1988. Compositional evolution of the zoned calcalkaline magma chamber of Mount Mazama, Crater Lake, Oregon. Contributions to Mineralogy and Petrology 98, 224–256.

Balesta, S.T., 1991. Earth crust structure and magma chambers of the area of present Kamchatka volcanism. In: Fedotov, S.A., Masurenkov, Y.P. (Eds.), Active Volcanoes of Kamchatka, vol. 1. Nauka, Moscow, pp. 166–197.

Barclay, J., Herd, R.A., Edwards, B.R., Christopher, T., Kiddle, E.J., Plail, M., Donovan, A., 2010. Caught in the act: implications for the increasing abundance of mafic enclaves during the recent eruptive episodes of the Soufrière Hills Volcano, Montserrat. Geophysical Research Letters 37, L00E09.

Belousov, A., Voight, B., Belousova, M., 2007. Directed blasts and blast-generated pyroclastic density currents: a comparison of the Bezymianny 1956, Mount St Helens 1980, and Soufrière Hills, Montserrat 1997 eruptions and deposits. Bulletin of Volcanology 69 (7), 701–740.

Bogoyavlenskaya, G.E., Braitseva, O.A., Melekestsev, I.V., Maximov, A.P., Ivanov, B.V., 1991. Bezymianny volcano. In: Fedotov, S.A., Masurenkov, Y.P. (Eds.), Active Volcanoes of Kamchatka, vol. 1. Nauka, Moscow, pp. 166–197.

Braitseva, O.A., Melekestsev, I.V., Bogoyavlenskaya, G.E., Maksimov, A.P., 1991. Bezymianny volcano: eruptive history and dynamics. Volcanology and Seismology 12, 165–195 (in Russian).

Churikova, T., Dorendorf, F., Worner, G., 2001. Sources and fluids in the mantle wedge below Kamchatka, evidence from across-arc geochemical variation. Journal of Petrology 42 (8), 1567–1593.

Class, C.D., Miller, D.M., Goldstein, S.L., Langmuir, C.H., 2000. Distinguishing melt and fluid subduction components in Umnak volcanics, Aleutian arc. Geochemistry, Geophysics, Geosystems 1 (Paper number 1999GC000010).

Couch, S., Sparks, R.S.J., Carroll, M.R., 2001. Mineral disequilibrium in lavas explained by convective self-mixing in open magma chambers. Nature 411, 1037–1039.

Donovan, J.J., Kremser, D., Fournelle, J.H., 2007. Probe for Windows User's Guide and Reference, Enterprise Edition, p. 355.

Eichelberger, J.C., Izbekov, P.E., Browne, B.L., 2006. Bulk chemical trends at arc volcanoes are not liquid lines of descent. Lithos 87 (1–2), 135–154.

Elliott, T., Plank, T., Zindler, A., White, W., Bourdon, B., 1997. Element transport from slab to volcanic front at the Mariana arc. Journal of Geophysical Research 102 (B7), 14991–15019.

Elsworth, D., Mattioli, G., Taron, J., Voight, B., Herd, R., 2008. Implications of magma transfer between multiple reservoirs on eruption cycling. Science 322, 246–248.

Fedotov, S.A., Zharinov, N.F., Gontovaya, L.I., 2010. The magmatic system of the Klyuchevskaya group of volcanoes inferred from data on its eruptions, earthquakes, deformation, and deep structure. Journal of Volcanolgy and Seismology 4, 3–32.

Girina, O.A., this issue. Chronology of Bezymianny Volcano activity, 1956–2010. Journal of Volcanology and Geothermal Research.

Grove, T.L., Elkins-Tanton, L.T., Parman, S.W., Chatterjee, N., Müntener, O., Gaetani, G.a, 2003. Fractional crystallization and mantle-melting controls on calc-alkaline differentiation trends. Contributions to Mineralogy and Petrology 145, 515–533.

Grove, T.L., Baker, M.B., Price, R.C., Parman, S.W., Elkins-Tanton, L.T., Chatterjee, N., Müntener, O., 2005. Magnesian andesite and dacite lavas from Mt. Shasta, northern California: products of fractional crystallization of H₂O-rich mantle melts. Contributions to Mineralogy and Petrology 148, 542–565.

Gust, D.A., Perfit, M.R., 1987. Phase relations of a high-Mg basalt from the Aleutian Island Arc: implications for primary island arc basalts and high-Al basalts. Contributions to Mineralogy and Petrology 97, 7–18.

Hildreth, W., 1983. The compositionally zoned eruption of 1912 in the Valley of Ten Thousand Smokes, Katmai National Park, Alaska. Journal of Volcanology and Geothermal Research 18, 1–56.

Hildreth, W., Moorbath, S., 1988. Crustal contributions to arc magmatism in the Andes of Central Chile. Contributions to Mineralogy and Petrology 98, 455–489.

Izbekov, P.E., Eichelberger, J.C., Ivanov, B.V., 2004. The 1996 eruption of Karymsky volcano, Kamchatka: historical record of basaltic replenishment of an andesite reservoir. Journal of Petrology 45, 2325–2345.

Kadik, A.A., Maksimov, A.P., Ivanov, B.V., 1986. Physico-chemical Conditions for Crystallization of Andesites. Nauka, Moscow, p. 158 (in Russian).

Kent, A.J.R., Darr, C., Koleszar, A.M., Salisbury, M.J., Cooper, K.M., 2010. Preferential eruption of andesitic magmas through recharge filtering. Nature Geoscience 3 (9), 631–636.

Koulakov, I., Gordeev, E.I., Dobretsov, N.L., Vernikovsky, V.A., Senyukov, S., Jakovlev, A., 2011. Feeding volcanoes of the Kluchevskoy group from the results of local earthquake tomography. Geophysical Research Letters 38, L09305.

Liu, T.C., Chen, B.R., Chen, C.H., 2000. Melting experiment of a Wannienta basalt in the Kuanyinshan area, northern Taiwan, at pressures up to 2.0 GPa. Journal of Asian Earth Sciences 18, 519–531.

Malyshev, A.I., 2000. Life of the Volcano. Ural Branch of Russian Academy of Sciences, Ekaterinburg (in Russian).

Melekestsev, I.V., Khrenov, A.P., Kozhemyaka, N.N., 1991. The tectonic setting and a general review of volcanoes in the northern group and in the Sredinnyi range. In: Fedotov, S.A., Masurenkov, Y.P. (Eds.), Active Volcanoes of Kamchatka, vol. 1. Nauka, Moscow, pp. 74–81.

Miesch, A.T., 1980. Scaling variables and interpretation of eigenvalues in principal component analysis of geologic data. Journal of the International Association for Mathematical Geology 12, 523–538.

Newman, S., Lowenstern, J.B., 2002. VolatileCalc: a silicate melt–H₂O–CO₂ solution model written in Visual Basic for excel. Computers & Geosciences 28, 597–604.

Pallister, J.S., Hoblitt, R.P., Crandell, D.R., Mullineaux, D.R., 1992. Mount St. Helens a decade after the 1980 eruptions; magmatic models, chemical cycles, and a revised hazards assessment. Bulletin of Volcanology 54, 126–146.

Pallister, J.S., Hoblitt, R.P., Meeker, G.P., Knight, R.J., Siems, D.F., 1996. Magma mixing at Mount Pinatubo; petrographic and chemical evidence from the 1991 deposits. In: Newhall, C.G., Punongbayan, R. (Eds.), Fire and Mud; Eruptions and Lahars of Mount Pinatubo, Philippines. University of Washington Press, Seattle, pp. 687–732.

Pallister, J.S., Thornber, C.R., Cashman, K.V., Clynne, M.A., Lowers, H.A., Mandeville, C.W., Brownfield, I.K., Meeker, G.P., 2008. Petrology of the 2004–2006 Mount St. Helens lava dome-implications for magmatic plumbing and eruption triggering.

In: Sherrod, D.R., Scott, W.E., Stauffer, P.H. (Eds.), A Volcano Rekindled: The Renewed Eruption of Mount St. Helens, 2004–2006: U.S. Geolog. Surv. Prof. Pap. p. 1750.

Plank, T., Langmuir, C.H., 1988. An evaluation of the global variations in the major element chemistry of arc basalts. Earth and Planetary Science Letters 90, 349–370.

Plechov, P.Y., Tsai, A.E., Shcherbakov, V.D., Dirksen, O.V., 2008. Opacitization conditions of hornblende in Bezymyannyi volcano andesites (March 30, 1956 eruption). Petrology 16, 19–35.

Ridolfi, F., Renzulli, A., 2012. Calcic amphiboles in calc-alkaline and alkaline magmas: thermobarometric and chemometric empirical equations valid up to 1,130 °C and 2.2 GPa. Contributions to Mineralogy and Petrology 163 (5), 877–895.

Ridolfi, F., Puerini, M., Renzulli, A., Menna, M., Toulkeridis, T., 2008. The magmatic feeding system of El Reventador volcano (Sub-Andean zone, Ecuador) constrained by texture, mineralogy and thermobarometry of the 2002 erupted products. Journal of Volcanology and Geothermal Research 176, 94–106.

Ridolfi, F., Renzulli, A., Puerini, M., 2010. Stability and chemical equilibrium of amphibole in calc-alkaline magmas: an overview, new thermobarometric formulations and application to subduction-related volcanoes. Contributions to Mineralogy and Petrology 160, 45–66.

Rock, N.M.S., Leake, B.E., 1984. The International Mineralogical Association amphibole nomenclature scheme: computerization and its consequences. Mineralogical Magazine 48, 211–227.

Scott, V.D., Love, G., Reed, S.J.B., 1995. Quantitative Electron-Probe Analysis. Ellis Horwood Limited, Hemel Hempstead, Hertfordshire, England, p. 311.

Shcherbakov, V.D., Plechov, P.Y., 2010. Petrology of mantle xenoliths in rocks of the Bezymyannyi Volcano (Kamchatka). Doklady Earth Sciences 434, 1317–1320.

Shcherbakov, V.D., Plechov, P.Y., Izbekov, P.E., Shipman, J.S., 2011. Plagioclase zoning as an indicator of magma processes at Bezymianny Volcano, Kamchatka. Contributions to Mineralogy and Petrology 162, 83–99.

Sparks, R.S.J., Sigurdsson, H., Wilson, L., 1977. Magma mixing: a mechanism for triggering acid explosive eruptions. Nature 267, 315–318.

Streck, M.J., Dungan, M.A., Malavassi, E., Reagan, M.K., Bussy, F., 2002. The role of basalt replenishment in the generation of basaltic andesites of the ongoing activity at Arenal volcano, Costa Rica: evidence from clinopyroxene and spinel. Bulletin of Volcanology 64, 316–327.

Sun, Shen-su, McDonough, W.F., 1989. Chemical and isotopic systematics of oceanic basalts: implications for mantle composition and processes. In: Saunders, A.D., Norry, M.J. (Eds.), Magmatism in the Ocean Basins: Spec. Publ. Vol. Geol. Soc. Lond., 42, pp. 313–345.

Thelen, W., West, M.E., Senyukov, S., 2010. Seismic characterization of the Fall 2007 eruptive sequence at Bezymianny Volcano, Russia. Journal of Volcanology and Geothermal Research 194, 201–213.

Timerbaeva, K.M., 1967. The Petrology of Kliuchevskoi Group of Volcanoes. Nauka, Moscow (in Russian).

Tindle, A.G., Webb, P.C., 1994. Probe-AMPH: a spreadsheet program to classify microprobe-derived amphibole analyses. Computers & Geosciences 20, 1201–1228.

Weltje, G.J., 1997. End-member modeling of compositional data: numerical–statistical algorithms for solving the explicit mixing problem. Mathematical Geology 29, 503–549.

Zellmer, G.F., Hawkesworth, C.J., Sparks, R.S.J., Thomas, L.E., Harford, C.L., Brewer, T.S., Loughlin, S.C., 2003. Geochemical evolution of the Soufrière Hills Volcano, Montserrat, Lesser Antilles volcanic arc. Journal of Petrology 44, 1349–1374.